A comparative study of flight performance of traditional and novel UAV platforms

Yuxiao Liu

Supervisor: Professor Meyer Nahon

Department of Mechanical Engineering

McGill University

A thesis submitted to McGill University in partial fulfilment of the requirements of the Undergraduate Honours Program.

Abstract

In this thesis, a framework is developed to compare flight performances of Unmanned Aerial Vehicles (UAVs) with different platform designs. A total of five UAV platforms are selected over a broad range: Traditional platforms including pure fixed-wing and rotary-wing aircraft, and novel hybrid platforms including body-sitter and tail-sitter. The selected prototypes are firstly scaled to a uniform dimension. Then a mission task that includes a complete return flight with multiple turning maneuvers is theoretically performed by all five UAV prototypes. This mission is performed under three conditions: their respective optimal operation points, a uniform high speed operation point, and a uniform low speed operation point. All UAVs' flight performances with respect to endurance, efficiency and maneuverability are then quantitatively compared. The results of this comparative study indicate that one of the selected hybrid prototypes, the VOGI, demonstrates the best performance under all three conditions, and therefore becomes the best platform design considered in this study.

Abrégé

Dans cette thèse, un cadre est développé pour comparer les performances de vol de véhicules aériens sans pilote (UAV) avec différentes conceptions de plates-formes. Au total, cinq plates-formes d'UAV sur lesquelles portent ces travaux sont sélectionnées parmi une vaste gamme: des plates-formes traditionnelles composées d'avions à voilure fixe et à voilure tournante purs et de nouvelles plates-formes hybrides composées de garde du corps et de queue. Les prototypes sélectionnés sont d'abord dimensionnés à une dimension uniforme, puis une tâche de mission comprenant un vol aller-retour complet avec plusieurs manœuvres de virage est théoriquement réalisée par les cinq prototypes de choix d'UAV sous trois conditions: leurs points de fonctionnement optimaux respectifs, une point de fonctionnement uniforme à haute vitesse et point de fonctionnement uniforme à basse vitesse. Les performances de vol de tous les UAV en termes d'endurance, d'efficacité et de maniabilité sont ensuite comparées quantitativement. Les résultats de cette étude comparative indiquent que l'un des prototypes hybrides sélectionnés, VOGI, présente la meilleure performance dans les trois conditions et qu'il devient par conséquent la meilleure conception de plate-forme dans cette étude.

Table of Contents

Acknowledgement

I would like to express my gratitude to my supervisor, Professor Meyer Nahon for the guidance, feedback, and the opportunity to work on this project. I would also like to thank Romain Chiappinelli for his help and advice. Lastly I want to thank the VOGI capstone design team for the inspiration in performance characterization methodology for hybrid aerial platforms.

Chapter 1: Introduction

1.1 Background and motivation

During the past two decades, Unmanned Aerial Vehicles have experienced tremendous development. Nowadays, most unmanned aerial vehicles can be separated into traditional horizontal take-off and landing aircraft, which are essentially referred to as fixed-wing aircraft, traditional vertical Take-Off and Landing (VTOL) aircraft, which are essentially referred to as rotary-wing aircraft, and hybrid VTOL UAVs. Each platform has its inherent advantages and limitations: Fixed-wing aircraft are efficient for long-distance transit flight but not very maneuverable, while rotary-wing aircraft feature maneuverability but lack in cruising efficiency. More recent novel hybrid UAVs, however, are believed to combine advantages of both of the conventional designs, allowing vertical take-off, hovering, and efficient cruising flight.

It is believed that the advantage of hybrid UAVs will result in their domination of the miniature UAV market [1]. Therefore, a work to analytically study their flight performance in comparison with traditional platforms becomes important.Hybrid UAVs typically have higher design and building cost, and more complicated control strategy, in comparison with conventional fixed-wing and multi-rotors UAVs in the market, making it important to quantify their potential advantages.

1.2 Brief categorization of UAV platform designs

As previously discussed in Section 1.1, UAVs can be first categorized into traditional horizontal take-off and landing aircraft (fixed-wing aircraft) and VTOL aircraft. VTOL aircraft can be further categorized into rotorcraft and hybrid UAVs. Starting from this point, current popular hybrid platform designs can be separated into a handful of subcategories. For this work, the classification is derived from [1], and is shown graphically in Fig 1-1.

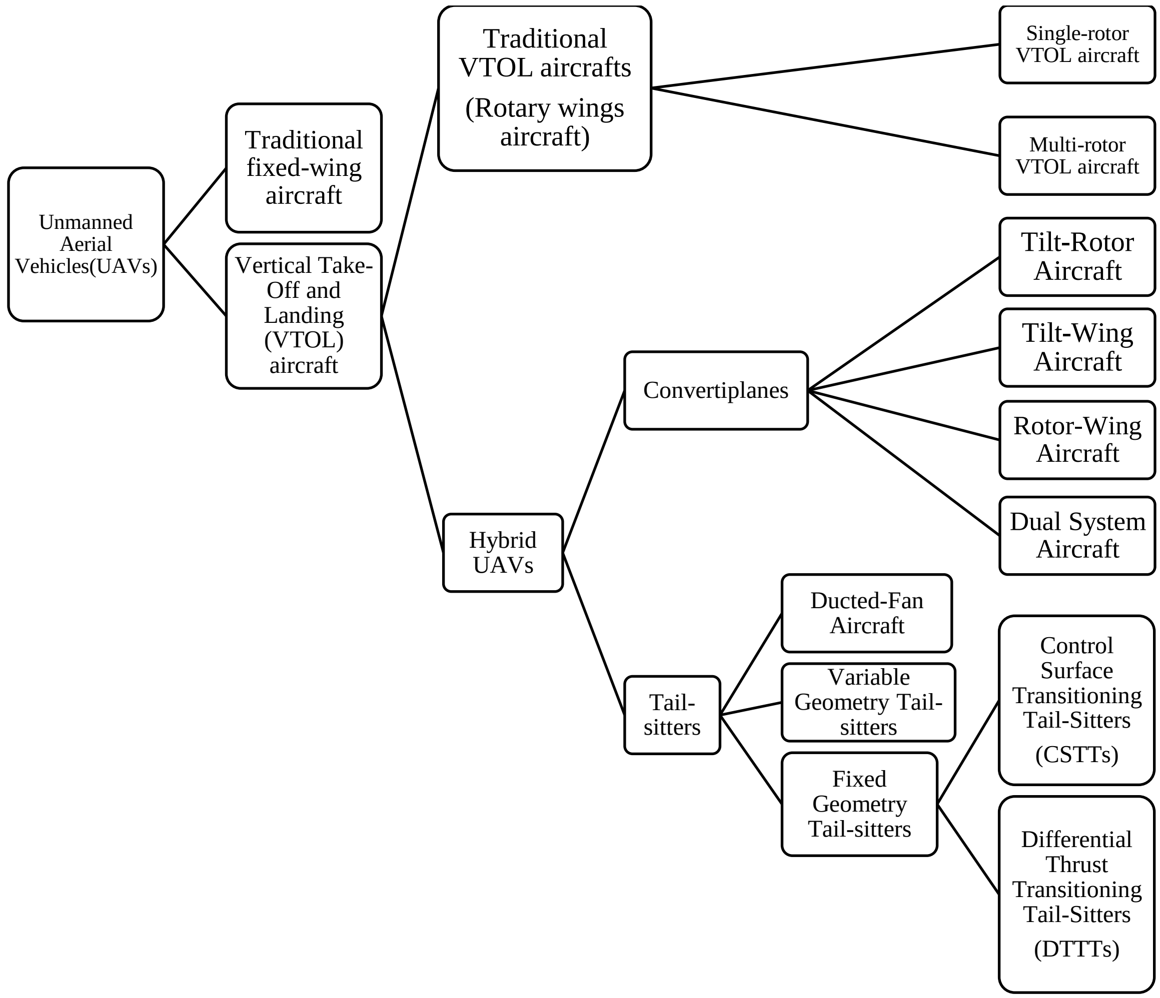

Figure 1-1: Classification of UAV platform designs

1.3 Choices of platform prototypes

Since it was not possible to analyze all the platforms shown in Fig. 1-1, we selected a subset that would cover a range of designs. This section provides reasoning for converging to particular UAV platforms listed in Fig. 1-1, and description of selected platform prototypes. As stated in Section 1.1, we hypothesize that hybrid UAVs, which inherit both VTOL ability as well as high cruising speed and enhanced endurance, may give better flight efficiency than traditional fixed-wing and rotary-wing aircraft. To act as a reference basis for our comparison study, one prototype is to be chosen from each category of fixed-wing and rotary-wing aircraft, and the rest will be chosen from hybrid UAVs category. To bring diversity to the platforms being compared, one prototype is chosen from each sub-category of hybrid UAVs, namely, convertiplanes and tail-sitters.

At this point, in order to proceed the selection with abundant sub-categories, certain additional criteria are considered. These criteria include the research and application popularity as well as flight efficiency prospective. These two criteria are considered in sequence until reaching final selections.

Research and application popularity: To make this comparison work significant, preference is given to mature and well-developed platform designs. Their popularity can be measured by number of written documents as well as manufactured prototypes. In this sense, the more prevalent multi-rotor VTOL design is preferred over single-rotor helicopters; Ducted-fan and variable geometry tail-sitters are removed from consideration due to the fact that no successful full envelope flight test has been conducted [1]. Finally, rotor-wing aircraft, is a platform that attracts relatively low research interests, have therefore been excluded from this study.

Flight efficiency prospective: In order to perform an impartial comparison, the remaining platforms are screened by selecting those with best-anticipated flight efficiencies, based on qualitative analysis. In the category of tail-sitters, although differential thrust transitioning tail-sitters can be significantly more stable in takeoff, hovering, and landing, they are also less efficient in horizontal flight compared to control surface transitioning tail-sitters due to extra rotors required to realize transition. Dual system convertiplanes will have relatively poor performance since the unused system gives no work but only adds weight and drag; Comparing tilt-rotor and tilt-wing aircrafts can be difficult, but one difference to be noticed is that most tilt-rotor aircraft feature a fly-wing configuration, which increases the wing area and therefore the lift generated. However, this design is physically impossible for tilt-wing aircraft to adopt, and thus, the tilt-rotor aircraft are determined to be more preferable to tilt-wing aircrafts.

The final list of selected platform designs is therefore: (1) traditional fixed-wing aircrafts, (2) traditional rotary-wing aircrafts, (3) tilt-rotor convertiplanes, and (4) control surface transitioning tail-sitters. Apart from the classifications listed in Fig 1-1, a decision is made to include one additoinal hybrid UAV prototype denoted as a passively-coupled tilt-rotor aircraft. This platform does not strictly fall under any subcategory, but is included to give more breadth to this study. A detailed description of the prototypes chosen for each type of platform is given in following sub-sections, along with their kry technical characteristics.

1.3.1 The Senior Telemaster Almost Ready to Fly (STARF)

The STARF (Fig. 1-2) is a fixed wing UAV developed by Hobby Lobby International, Inc. [2]. It is constructed of balsa and hardwoods, with a rib and spar wing. A commonly seen fixed-wing and tractor configuration makes STARF a suitable reference aircraft to be adopted. Selected technical parameters are provided in Table 1-1.

Parameter	Value	Unit
Wingspan	2.38	m
Wing planform area	0.858	m^2
Length	1.625	m
Height	0.55	m
Take-off Mass	12.56	kg
Rotor diameter	0.381	m

Table 1-1: STARF Parameters, No payload [2]

Figure 1-2: STARF

1.3.2 Valkyrie

Valkyrie is a hexacopter rotary-wing UAV developed by AeroMcGill Drones team, and it has been used for Unmanned Systems Canada (USC) student drone design competition [3]. The reason why Valkyrie is chosen lies in its hexacopter configuration, which is not common in rotary-wing UAV regime, and will avoid partially structural overlap with some certain hybrid UAVs that incorporate quadrotor designs.

Parameter	Value	Unit
Rotor diameter	0.457	m
Length	1.5	m
Take-off Mass	5.6	kg
Rotor blade average chord	0.038	m
Rotor blade pitch	0.14	m

Table 1-2: Valkyrie Parameters, No payload [3]

Figure 1-3: Valkyrie

1.3.3 X-VERT

X-VERT (Fig. 1-4) is an agile, fixed geometry control surface transitioning tail-sitter (CSTT) developed by Horizon Hobby. This is a flying wing aircraft that takes off and lands nose up. In order to perform the transition from hovering flight, the entire aircraft needs to pitch down to enter level flight [4]. X-VERT's configurational simplicity and lower cost make it a suitable platform for this project to use.

Parameter	Value	Unit
Wingspan	0.5	m
Wing planform area	0.0798	m^2
Length	0.264	m
Take-off mass	0.21	kg
Rotor diameter	0.125	m

Table 1-3: X-VERT Parameters, No payload [4]

Figure 1-4: X-VERT

1.3.4 FireFLY 6

The FireFLY6 (Fig. 1-5) is a tilt rotor design incorporating a flying wing with three counter-rotating thruster pairs. During vertical maneuvers, the airplane works like a tricopter with all of its three sets of coaxial-rotors pointing vertically. In order to perform transition to level flight, the two front thrust pairs start to tilt forward. As the aircraft gains forward speed, lift is generated by the wings and the rotors are eventually tilted fully forward providing longitudinal thrust to maintain speed.

The tilt-rotor body-sitter, also referred to as convertiplane, features relatively no attitude change between take-off, hover, and cruise phases. In other words, the wing and fuselage of a convertiplane remain parallel to the ground during the entire flight. This attitude difference in vertical and transition maneuver between convertiplanes and tail-sitters makes the FireFLY6 a good comparison to be selected for this project.

Parameter	Value	Unit
Wingspan	1.524	m
Wing planform area	0.64	m²
Length	0.828	m
Take-off mass	4.5	kg
Rotor diameter	0.255	m

Table 1-4: FireFLY 6 Parameters, No payload [5]

Figure 1-5: FireFLY 6

1.3.5 VOGI

VOGI is known as a Pitch-Decoupled Tilt Rotor, or alternatively, Passively-Coupled Tilt Rotor VTOL aircraft. It proposes a system that passively couples a quadrotor to a fixed-wing airframe about the pitch axis. This allows independent pitch rotation of the two airframes relative to each other, and is claimed to result in a more stable transitional phase as compared to traditional tilt-rotor aircraft, which require actuators to actuate the tilting mechanisms. Furthermore, with the bidirectional rotor installed at the rear of the aircraft, the pitch angle at low speed is well controlled.

Although VOGI cannot be separated into any specific sub-categories listed in Fig. 1-1, it is included here for its design uniqueness, as well as the fact that a proof-of-concept VOGI aircraft has been successfully flown, and a better efficiency in cruising regime is promising [6].

Parameter	Value	Unit
Wingspan	1	m
Wing planform area	0.14	m^2
Rotor diameter	0.127	m
Take-off mass	1	kg

Table 1-5: VOGI Parameters, No payload [6]

Figure 1-6: VOGI, hovering mode

1.4 Thesis objective and overview

This thesis aims to develop methodologies to quantify the endurance, efficiency and maneuverability of different UAV designs, and to develop a framework to compare performance metrics of selected novel and traditional UAV prototypes.

The motivation for this study, platform categorization and prototypes selection have been discussed in Chapter 1. Chapter 2 introduces the comparison framework including prototype scaling and mission task description. The calculation methodology of performance metrics for different platforms is covered in Chapter 3, and the final results of this study are presented in Chapter 4, along with discussion and comments. Chapter 5 summarizes the comparison work and discusses potential future work.

Chapter 2: Comparison framework

2.1 Mission task and competition description

2.1.1 Mission task description

In order to analyze the flight efficiency of an aircraft, a mission task comprising a complete flight course is established. As shown in Fig. 2-1, the aircraft departs at a start point and performs a steady, level cruising flight until entering the survey area, where a monitoring task is to be conducted. This objective can be realized by performing 'lawn-mower' movements, that is, to make 180° turn when reaching the boundary of the survey area, and continue until the survey is finished. After exiting the survey area the aircraft follows another straight line, and cruises back to the start point to end the mission task.

The distance from start point A to B is AB = 1.5 km, and the survey area width BC = 1 km. The survey area is expansive enough that can be assumed to be extending into infinity in length, as seen in Fig. 2-1. The red shadowed area is taken to be the observable area each time the aircraft pass through, and assuming the required survey tasks can be carried out under a maximum radius of 20 m, the width of observed area becomes 40 m. The mission task comes with a recommended cruising height of $H = 30\ m$, due to the safety concern brought by potential terrains in the survey area. The start point A is taken to be the point where all prototypes start cruising, therefore a runway is incorporated before point A for STARF's use.

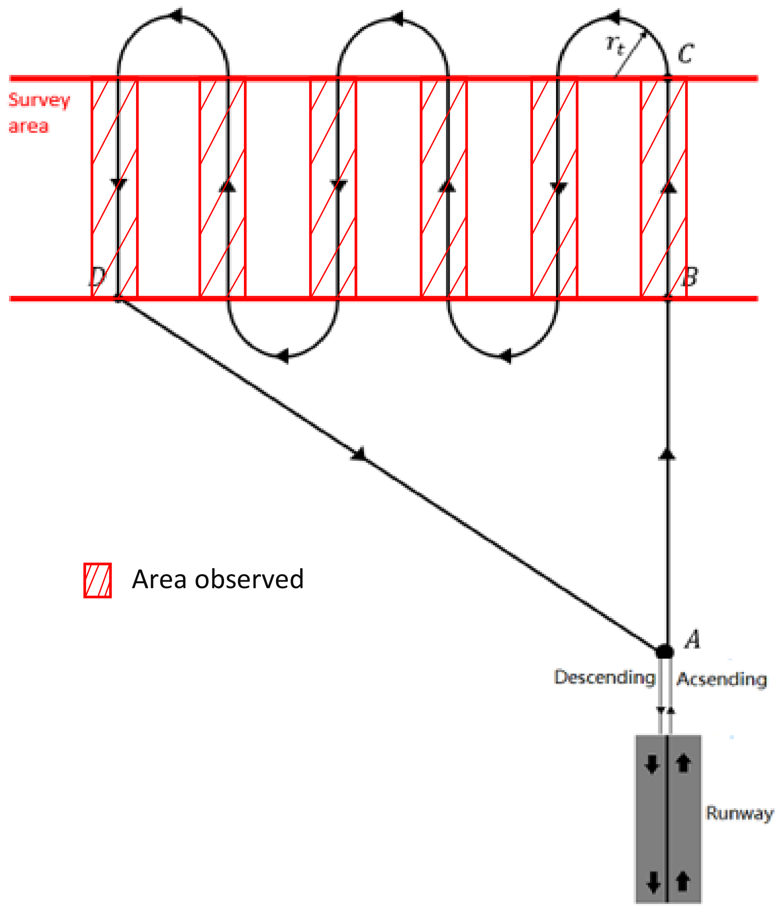

Figure 2-1: Mission task visualization

2.1.2 Competition descriptions

The competition is set up to be in two parts. The first competition (competition #1) essentially exploits all available energy of an aircraft, with 10% energy remaining as safety margin. In this competition each aircraft operates at its optimum condition calculated in Chapter 4, i.e., cruising at the velocity that generates maximum range, and performing turns at the velocity that generates shortest radius of turn. The number of turns made depends on the remaining available energy. The total observed area, area ratio, full-envelope average speed, and energy consumption per distance are to be compared. The area ratio is defined as the ratio of area observed to area explored, which can be calculated as:

$$Area\ explored = (BD + 40\ m)BC$$

The second competition (competition #2) is more standardized, where all of the five prototypes are to be operated at the same cruising speed, with a prescribed number of turns to make. The comparison criteria will be energy consumption per distance, radius of turn or area ratio, as well as time required to finish the mission task. Detailed metrics used in this competition are to be determined after the optimum condition performance metrics are calculated in Chapter 4.

2.2 Payload selection

Considering the size and capability of selected prototypes, as well as the exploratory nature of the mission task to be carried out, a compact stabilized sensor payload with high image resolution is sought. After a survey of various options, the MICRO-STAMP miniature payload developed by CONTROP Precision Technologies Ltd. is considered to be ideal. The MICRO-STAMP weighs 0.32kg, and its power consumption ($P_{Payload}$) is assumed to be 10W based on that of an average security camera (8W)

Figure 2-2: Payload of selection: MICRO-STAMP

2.3 Prototypes scaling methodology

After platform prototypes are selected as discussed in Section 1.3, we ensure a fair and valid comparison between them by first scaling the various aircraft prototypes to a uniform dimension.

By referring to rules of different international drone design competitions, the aircrafts are restricted in a way that the wingspan should not exceed 5 ft (1.524 m). These restrictions are adapted from the rules of AI Drone 2017 UAV Competition hosted by The University of Tulsa [7]. In the case of Valkyrie, where wingspan is not an applicable parameter, the aircraft length is used instead.

The length scaling factor k can be expressed as:

$$k = \frac{l_{original}}{l_{scaled}}$$

Where $l_{original}$, l_{scaled} are original and scaled characteristic length. For geometrically similar objects it holds that $W \propto l^3$, where W is the weight. Therefore one can write:

$$k^3 = \frac{W_{original}}{W_{scaled}}$$

In the case of rotary-wing aircraft, or more specifically Valkyrie in this case, regression analysis has shown the relationship between rotor diameter, $d_{rotor,eq}$, and takeoff mass, M_{TO}, is given by [8]:

$$d_{rotor,eq} = \alpha(M_{TO})^{0.4}$$

Note that the $d_{rotor,eq}$ here is the equivalent rotor diameter that correponds to total rotor disk area. Now the rotor diameter scaling factor c can be expressed as:

$$c = \frac{\sqrt{N}d_{rotor,original}}{\sqrt{N}d_{rotor,scaled}} = \frac{d_{rotor,eq,original}}{d_{rotor,eq,scaled}} = (\frac{M_{original}}{M_{scaled}})^{0.4} = (\frac{W_{original}}{W_{scaled}})^{0.4}$$

Where N is the number of rotors. Therefore to scale Valkyrie both k and c will be used. i.e., length and mass will be scaled by k, and rotor quantities will be scaled by c. The original size and weight of the 5 prototypes varies greatly from each other, and in some cases it is unrealistic to impose the payload of choice to a given aircraft. For example, the take-off mass of X-VERT (0.21kg) is smaller than that of the payload. Therefore payload mass is incorporated after the aircraft are scaled. Parameters of scaled prototypes are shown in Table 2-1 to Table 2-5 along with scaling factors adopted.

Parameter	Value	Unit
Wingspan	1.524	m
Wing planform area	0.351	m^2
Length	1.04	m
Height	0.352	m
Take-off Mass	3.62	kg
Rotor diameter	0.244	m

Table 2-1: Scaled STARF Parameters, with payload, k=1.5616

Parameter	Value	Unit
Rotor diameter	0.466	m
Length	1.524	m
Take-off Mass	6.19	kg
Rotor blade average chord	0.039	m
Rotor blade pitch	0.143	m

Table 2-2: Scaled Valkyrie parameters, with payload, k=0.9842, c=0.9810

Parameter	Value	Unit
Wingspan	1.524	m
Wing planform area	0.74	m^2
Length	0.804	m
Take-off mass	6.26	kg
Rotor diameter	0.381	m

Table 2-3: Scaled X-VERT parameters, with payload, k=0.3281

Parameter	Value	Unit
Wingspan	1.524	m
Wing planform area	0.64	m^2
Length	0.828	m
Take-off mass	4.82	kg
Rotor diameter	0.255	m

Table 2-4: Scaled FireFLY 6 parameters, with payload, k=1

Parameter	Value	Unit
Wingspan	1.524	m
Wing planform area	0.325	m^2
Rotor diameter	0.193	m
Take-off mass	3.86	kg

Table 2-5: Scaled VOGI parameters, with payload, k=0.6561

Chapter 3: Flight performance metrics evaluation

The performance metrics for all the five prototypes are calculated here under the optimal flight condition, which is the maximum flight range and shortest radius of turn. These conditions are set up due to the exploration requirement of the mission task. It is important to note that the conditions for maximum flight range are not equivalent to those for maximum endurance. Once the evaluation methodology is established it will be possible to evaluate the performance metrics under any flight condition, given sufficient known inputs.

3.1 Power source selection and calculation

To start with, the power source is to be selected. Based on the uniform UAV frame size of 1.524 m and the corresponding recommendation from [9], the power source selected is a 6-cells 8000mAh Li-Po battery pack, with 22.2V and 150C rating. The Peukert's equation [10] with discharge rate effect incorporated reads

$$t = \frac{R_t}{i^n}\left(\frac{C}{R_t}\right)^n \tag{3.1}$$

where t is time in hours, R_t is battery hour rating, and is typically one hour for small rechargeable battery packs [11]. C is capacity in ampere hours, i is the discharge current, n is the discharge parameter and is taken to be 1.3 [11] for Li-Po batteries. Combining with the electrical power output $P_B = V_r i$ yields:

$$P_B = V_r \frac{C}{R_t}\left(\frac{R_t}{t}\right)^{\frac{1}{n}} \tag{3.2}$$

where P_B is the battery power supplied, and V_r is the rated voltage.

3.2 Cruising performance evaluation

3.2.1 Fixed-wing aircraft, STARF

For a fixed-wing aircraft in steady cruising flight, the lift and drag forces are:

$$L = W = \frac{1}{2}\rho V^2 S C_L \tag{3.3}$$

$$D = T = \frac{1}{2}\rho V^2 S C_D \tag{3.4}$$

Where S is the wing planform area. The drag coefficient expressed as drag polar is:

$$C_D = (k{C_L}^2 + C_{D_0})(1 + DF) \tag{3.5}$$

Where DF is the drag factor due to the addition of items to the airframe, which then reduces aircraft's 'cleanness' and increases the drag. The value of drag factor is then evaluated on the basis of the influences brought by different added items as listed in Table 3-1. Note that different aircraft configurations will come with different combinations of items.

Drag items	Drag Factor
1.Antenna installation	4.8%
2.Gap in control surfaces	2.76%
3. Landing gear assembly installation	4.43%
4. Wing irregularities and leakage	5.95%

Table 3-1: Drag item and its corresponding Drag increment [12] [13]

The required power for cruising can be expressed as:

$$P_{req} = \frac{DV}{\eta_{tot}} \tag{3.6}$$

where η_{tot} is the total efficiency of the propeller-motor combination. Wind tunnel tests with a typical Mega 16/15/6 brushless drone motor and a 7*4 propeller have shown an average value of $\eta_{tot} = 0.5$ [14]. Combining (3.6) with (3.3) (3.4) (3.5) the equation becomes:

$$P_{req} = \frac{\frac{1}{2}\rho V^3 S C_{D_0} + \frac{2W^2 k}{\rho V S}}{\eta_{tot}}(1 + DF) \tag{3.7}$$

Since the power supplied by the batteries is considered as the total available power for an aircraft, the following relation will hold:

$$P_B = P_{req} + P_{payload} + P_{avionics} \tag{3.8}$$

As specified before in Section 2.2, $P_{payload}$ is taken to be 10 W. The Valkyrie's avionics system is composed of Pixhawk 2.1 standard set, whose rated peak power draw is 3A at 5V [15]. Therefore the avionics system power consumption, $P_{avionics}$, is assumed to be 15 W for Valkyrie as well as for the four other prototypes for the purpose of this comparative study. One can now combine equations (3.2) and (3.8) and rearrange to obtain the expression of endurance, E.

$$E = t = R_t^{1-n} \left[\frac{V_r C}{P_{req} + P_{payload} + P_{avionics}} \right]^n \tag{3.9}$$

The condition for maximum range occurs at the minimum drag condition, which can be derived from (3.5). That is,

$$C_{D_0} = k{C_L}^2 \xrightarrow{yields} V_R = \sqrt{\frac{2W}{\rho S} \sqrt{\frac{k}{C_{D_0}(1 + DF)}}} \tag{3.10}$$

where V_R is the velocity that yields maximum range. Note that here the $(1 + DF)$ term is added manually to once again account for the drag factor correction. To estimate maximum range, substitute V_R into (9) to obtain the time aloft, and the range is given by:

$$R_{max} = E(V_R)V_R \tag{3.11}$$

To perform the calculation one needs to determine C_{D_0}, the parasite drag coefficient, and k, the induced drag parameter. k can be calculated as:

$$k = \frac{1}{\pi e AR}$$

AR is aspect ratio and e is Oswald efficiency. Regression analysis shows that [16]:

$$e = \frac{1}{1.05 + 0.007\pi AR} \tag{3.12}$$

The parasite drag coefficient is evaluated as:

$$C_{D_0} = C_{fe}\frac{S_{wet}}{S} \tag{3.13}$$

Where S_{wet} is the total wetted area. The break-down of S_{wet} as well as estimation of its value based on aircraft configuration for all five prototypes except Valkyrie is tabulated in Table 3-2:

	STARF	X-VERT	FireFLY6	VOGI
$S_{fuselage}$	$(0.7S) \times 2$	$(0.15S) \times 2$	$(0.35S) \times 2$	$(0.4S) \times 2$
S_{wing}	$2S$	$2S$	$2S$	$2S$
$S_{vertical\ tail}$	$(0.5S) \times 2$	___	___	___
$S_{horizontal\ tail}$	$(0.2S) \times 2$	___	___	$(0.15S) \times 2$
$S_{quad\ airframe}$	___	___	___	$(0.1S) \times 2$
Total	$4.8S$	$2.3S$	$2.7S$	$3.3S$

Table 3-2: Wetted area breakdown based on wing planform area for all prototypes except Valkyrie

Where S is each aircraft's corresponding wing planform area, and values are doubled when both sides of surfaces are exposed to fluid. Regression analysis approximating C_{fe}, the equivalent skin friction coefficient, indicates that [17]:

$$C_{fe} = 0.00258 + 0.00102e^{(-6.28\times10^{-9}Re)} + 0.00295e^{(-2.01\times10^{-8}Re)} \tag{3.14}$$

A reasonable approximation is to assume the power of e to be zero, considering the Reynold's number the prototypes typically fly at (magnitude scale of 10^5~10^6, as supported by results in Chapter 4). This assumption leads to a C_{fe} value of 0.0065.

3.2.2 Rotary-wing aircraft, Valkyrie

The power consumption in a rotary-wing aircraft is quite different than for a fixed-wing aircraft. In this case, we break down the total power required into parasite, induced and profile power required [13].

3.2.2.1 Parasite power, P_{para}

The drag force a rotorcraft has to overcome when moving through the air is evaluated as [18]:

$$D = (\frac{1}{2}\rho V^2 f_{fuse})(1 + DF) \tag{3.15}$$

Where DF is the drag factor as with fixed-wing aircraft, and f_{fuse} is the flat plate area attributable to the fuselage body. By looking at Valkyrie's CAD drawing packages and for the purpose of analyzing, Valkyrie's fuselage is modelled as a cube with a length (l_{fuse}) of 0.3 m. The drag coefficient C_d for bluff object typically ranges from 1.0 to 1.2 [13]. Assuming a C_d of 1.0, the equivalent flat plate area f_{fuse} becomes the fuselage frontal area of 0.09 m^2.

With drag force calculated in equation (3.15), the parasite power required to move Valkyrie through the air is then evaluated as:

$$P_{para} = DV = (\frac{1}{2}\rho V^3 f_{fuse})(1 + DF) \tag{3.16}$$

3.2.2.2 Induced power, P_{ind}

The induced power required to generate rotor thrust is obtained from Glauert's hypothesis [13]:

$$P_{ind} = T v_i \tag{3.17}$$

Where T is the thrust or weight. The theoretical value of P_{ind} represents an unattainable minimum value, which, based on experience, should be increased by 15% [19].

To obtain the induced velocity, v_i, we first evaluate the value of total velocity (vector sum of flight velocity and induced velocity), V', as follows:

$$V' = \sqrt{(v_i + Vsin\alpha)^2 + (Vcos\alpha)^2}$$

Where α is the angle-of-attack, and during steady level flight it is derived as:

$$\alpha = \sin^{-1}(\frac{D}{T})$$

Where D is as determined by equation (3.15). From rotor disk control volume analysis, the relation between rotor thrust T and induced velocity v_i can be deduced:

$$T = 2\dot{m}v_i = 2\rho A_r v_i V'$$

Where A_r is the total rotor disk area. Combining with the induced velocity under hovering case,

$$v_h = \sqrt{\frac{T}{2\rho A_r}}$$

Where T is thrust or weight. The final expression for induced velocity becomes:

$$v_i = \frac{{v_h}^2}{\sqrt{(v_i + Vsin\alpha)^2 + (Vcos\alpha)^2}} \quad (3.18)$$

Under a prescribed velocity V, equation (3.18) can be solved to evaluate v_i, which is then used to solve equation (3.17) to get the value of P_{ind}.

3.2.2.3 Profile power, P_{pro}

The profile power required to turn the rotor blades through the air is calculated as [13]:

$$P_{pro} = \rho A_r {V_T}^3 \frac{\sigma C_d}{8}(1 + 3\mu^2) \quad (3.19)$$

Where V_T is the blade tip speed defined as the product of rotor radius and rotor angular rotational speed. Under a typical operational motor throttle of 65% [3], Valkyrie's combination of MN5212 kV340 motor and 1855 propeller gives 4622 rpm [20]. The blade solidity, σ, is the ratio of blade average chord to the pitch length. C_d is the drag coefficient, and μ is the ratio between forward speed V and blade tip speed V_T.

Considering the flight regime of Valkyrie, which features low speed and therefore relatively low Reynold's number, the influence of choice of rotor blade airfoil on drag coefficient is minimal. Thus, a commonly-used NACA-4 digits airfoil can be assumed, and by sorting the maximum C_l/C_d the airfoil gives under Reynold's number of around 200,000, the NACA-6409 9% airfoil is finally fixed [21]. With the airfoil characteristic the following expression for C_d can be obtained:

$$C_d = 0.0037{C_l}^2 + 0.0025$$

Where the lift coefficient C_l can be determined as [13]:

$$C_l = \frac{6K_T}{\sigma(1 + \frac{3\mu^2}{2})}$$

Where K_T is the thrust coefficient associated with induced inflow ratio,

$$K_T = \frac{T}{\rho A_r {V_T}^2}$$

3.2.2.4 Total required power, P_{req}

To calculate the total power required by Valkyrie during steady forward flight, one can combine equation (3.16)(3.17)(3.19), that is,

$$P_{req} = \frac{1}{2}\rho V^3 f_{fuse}(1 + DF) + 1.15Tv_i + \rho A_r {V_T}^3 \frac{\sigma C_d}{8}(1 + 3\mu^2) \quad (3.20)$$

The expression of P_{req} is then a function of forward velocity V. To determine the endurance of Valkyrie with given power system parameters, equation (3.9) can be evaluated with P_{req} calculated from (3.20), and the range is then given by $R = EV$. The maximum range R_{max} and its corresponding V_R can be found by plotting the variation of R with V and finding the point where maximum R occurs. Substituting the resulting V_R back to equation (3.20) allows us to solve for P_{req} and E subsequently.

3.2.3 Hybrid aircraft

The hybrid UAV platforms included in this work, VOGI, FireFLY 6 and X-VERT, feature novel configurations that lead to their flight mechanics being inadequately covered by the specific cases of fixed-wing and rotary-wing aircrafts. For this reason, a flight performances evaluation method based essentially on propeller power consumption estimation is proposed, since it is assumed to be more efficient and accurate compared to methods adopted previously which generate performance metrics by accounting for all drag forces the aircraft is subject to.

To start with, the total propeller power consumption is evaluated as:

$$P_{req} = P_{prop} = n \cdot Q\omega = n \cdot (\frac{4}{\pi^3}\rho\omega^3 r^5 C_P) \tag{3.21}$$

Where Q is propeller torque, ω is propeller angular speed, C_P is power coefficient. A coefficient n is added manually to account for aircraft's total number of operating rotors during cruising flight. The value of ω under different flight operating points can be found from the expression for propeller thrust T:

$$T = n \cdot (\frac{4}{\pi^2}\rho\omega^2 r^4 C_T) \tag{3.22}$$

Where C_T is propeller thrust coefficient, and the value of T is determined from kinetics equations governing each aircraft's steady level flight. The power and thrust coefficients can be approximated by assuming their quadratic variation with advance ratio J [4], which is defined as:

$$J = \frac{\pi V}{\omega r}[1/rev] \tag{3.23}$$

To obtain the quadratic equations relating C_P and C_T with J, wind tunnel experiments can be performed, and data generated from such experiments are available at UIUC and APC propeller database. Using information given in Table 3-3, the relevant propellers are identified in the database, and the propeller coefficients variation with J is plotted and visualized in Fig. 3-1 through Fig. 3-3. Note that in order to include the influence of ω, the data for each propeller is extracted for different angular speed ranges from 5000 rpm to 10000 rpm and averaged, making the resulting plotted lines less smooth than anticipated.

Prototype	**Propeller equipped**	***n***
VOGI	GWS 5043	4
FireFLY 6	Aeronaut 1145	4
X-VERT	GWS 4530	2

Table 3-3: Types of propeller equipped and values of n

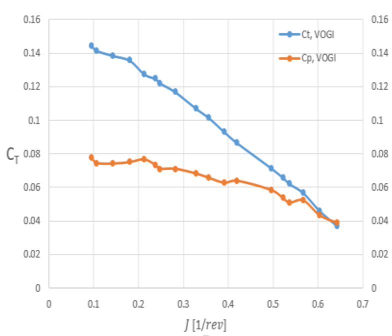

Fig 3-1: $C_P(J)$ and $C_T(J)$, VOGI

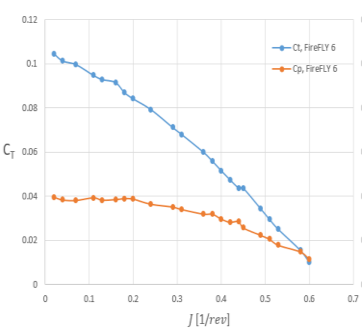

Fig 3-2: $C_P(J)$ and $C_T(J)$, FireFLY 6

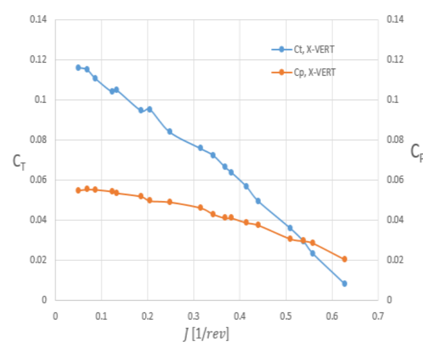

Fig 3-3: $C_P(J)$ and $C_T(J)$, X-VERT

With this data, we can find the best-fit quadratic equations for C_T and C_P. For VOGI, the resulting propeller coefficients as functions of the advance ratio are given as:

$$C_T(J) = -0.1091J^2 - 0.1180J + 0.1575$$

$$C_P(J) = -0.1102J^2 - 0.0160J + 0.0752$$

For FireFLY 6:

$$C_T(J) = -0.1305J^2 - 0.0819J + 0.1058$$

$$C_P(J) = -0.1123J^2 - 0.0241J + 0.0377$$

and for X-VERT:

$$C_T(J) = -0.1097J^2 - 0.1120J + 0.1213$$

$$C_P(J) = -0.0660J^2 - 0.0155J + 0.0566$$

For a given desired flight velocity, required thrust T can be determined from force analysis of each prototype. With T being calculated, equation (3.22) can now be solved to determine ω, and the required power P_{req} can be calculated subsequently from (3.21). To determine endurance equation (3.8) can be recast. The range is then given as $R = EV$, and the maximum range R_{max} and the corresponding speed V_R can be found from the plot of R against V.

Finally, the required propeller thrust T is to be determined from force analysis of each prototype, as detailed in following Sections 3.2.3.1 to 3.2.3.3.

3.2.3.1 VOGI

VOGI's flight attitude as well as its corresponding free body diagram is shown in Fig. 3-4, where θ is the rotor pitch angle and α is the angle of attack. During steady level flight the rear rotor is not operating to save power, and for convenience, the free body diagram can be recast as in Fig. 3-5. Applying the force balance in horizontal and vertical direction and replace the expression of lift and drag by equation (3.3) and (3.4)(3.5) one can obtain the following set of equations:

$$T\sin\theta = \frac{1}{2}\rho V^2 S(C_{D_0} + k{C_L}^2)(1 + DF) \tag{3.24}$$

$$T\cos\theta + \frac{1}{2}\rho V^2 S C_L = mg \tag{3.25}$$

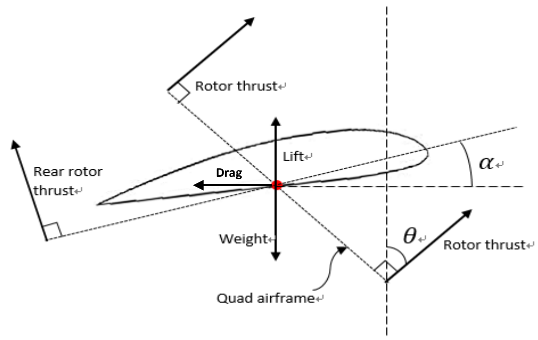

Fig 3-4: VOGI's FBD

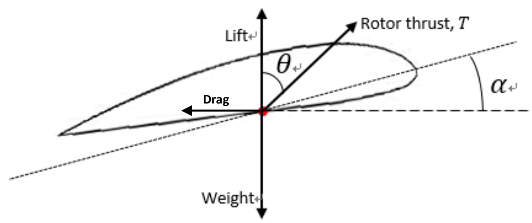

Fig 3-5: VOGI’s FBD for equivalent force analysis

Where the parasite drag coefficient C_{D_0} and linear extent k can be determined as in Section 3.2.1. Here the lift coefficient C_L is assumed to be changing linearly with α, that is:

$$C_L = C_{L,\alpha}\alpha \tag{3.26}$$

Using CFD techniques, VOGI’s design team has plotted the variation of C_L and α, and the linear function generated by regression analysis has shown a $C_{L,\alpha}$ value of 4.91 [22]. With each prescribed flight speed V, a value of α is randomly selected, and the equation set can be solved to generate θ and T. The generated results are then used to calculate the range R. The calculation procedure proceeds with next selection of α and stops when α reaches a critical value, which is taken to be 18° in this study. The flight condition (α, θ and T) at each velocity V is fixed at the point where the calculated R reaches a maximum.

3.2.3.2 FireFLY 6

FireFLY 6 is a tilt-rotor UAV with a fly-wing configuration. FireFLY 6’s flight attitude as well as its corresponding free body diagram is shown in Fig. 3-6, and under steady level flight FireFLY 6 can be analyzed with an identical equivalent forces diagram as VOGI, shown by Fig. 3-7.

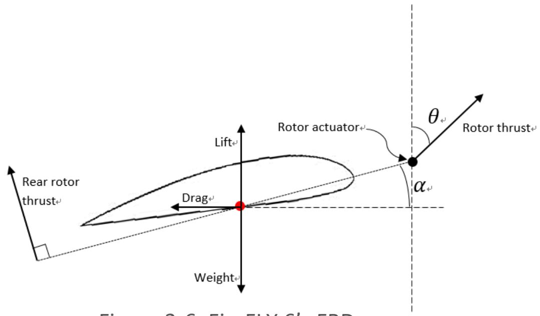

Figure 3-6: FireFLY 6's FBD

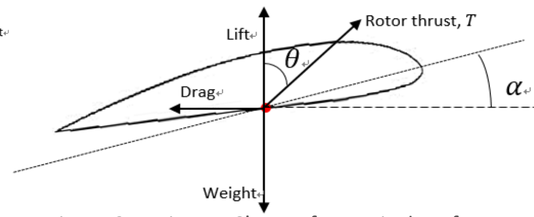

Figure 3-7: FireFLY 6's FBD for equivalent force analysis

The kinetics equations are then given by equations (3.24) and (3.25), with the lift coefficient C_L given by equation (3.26). For aircraft with a fly-wing configuration, the linear coefficient $C_{L,\alpha}$ can be calculated using the following approximation [4]:

$$C_{L,\alpha} = \frac{2\pi cos\Lambda}{\frac{2cos\Lambda}{AR} + \sqrt{1 + (\frac{2cos\Lambda}{AR})^2}} \tag{3.27}$$

Where Λ is the sweep angle of the fly-wing. As given by Fig. 3-8, the value of sweep angle can be approximated by $\Lambda = \tan^{-1}(\frac{0.6l}{0.3b}) = 47.37°$. With an aspect ratio of 3.629, the calculated $C_{L,\alpha}$ of FireFLY 6 becomes 2.96.

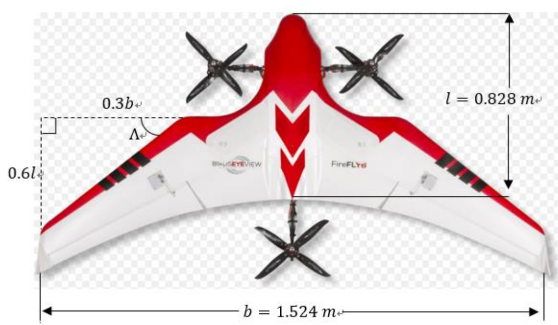

Figure 3-8: Sweep angle approximation, FireFLY 6

3.2.3.3 X-VERT

The X-VERT is a Control Surface Transitioning Tail-sitter (CSTT) with flying-wing configuration. Unlike tilt-rotor aircrafts, X-VERT cruises with its rotors pitched at the same angle as the aircraft's angle of attack, or pitch angle, since during level flight $\theta_{lvl} = \alpha$.

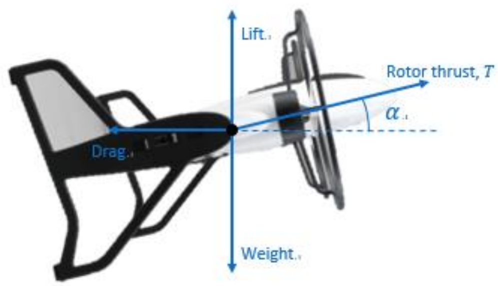

Figure 3-9: X-VERT's FBD for equivalent force analysis

From Fig. 3-9, the sum of forces along horizontal and vertical axis can be computed as:

$$T \sin \alpha + \frac{1}{2}\rho V^2 S C_L = mg \tag{3.28}$$

$$T \cos \alpha = \frac{1}{2}\rho V^2 S(C_{D_0} + k{C_L}^2)(1 + DF) \tag{3.29}$$

Where C_L is calculated using equation (3.26) and (3.27), and the sweep angle for X-VERT is given as 19.8° [4] and the aspect ratio is 3.138, yielding a $C_{L,\alpha}$= 3.35. As a result, for a given speed V, equation (3.28) and (3.29) contains 2 unknowns: rotor thrust T, and angle of attack α, and so can be solved directly.

3.3 Turning performance evaluation

The radius of turn, r_t, for an aircraft can be calculated from [13]:

$$r_t = \frac{{V_t}^2}{g tan\phi} \tag{3.30}$$

Where V_t is the aircraft's turning velocity and ϕ is the bank angle, which can be related to the load factor (ratio of thrust to weight), N, by the following equation:

$$N = \sqrt{1 + \tan^2 \phi} \tag{3.31}$$

The bank angle have to be maximized and the turning velocity have to be minimized in order to have a minimized radius of turn. The shortest radius of turn is also limited by the power required for turning $P_{t,req}$, which should not exceed P_{req} since the power source P_B is evaluated as in equation (3.8).

The US Federal Aviation Regulations specified for transport category airplanes a minimum load factor of 2.5 [23], and for the small-class UAVs except Valkyrie this thesis is dealing with, the load factor of 2.5 is assumed to be the safety limit; for Valkyrie it comes with a design load factor of 2.9 [3] and will then be adopted as the limit instead.

For STARF, the minimized V_t is taken to be 15% [19] above its stall speed V_{stall}, which is evaluated as:

$$V_{stall} = \sqrt{\frac{W}{\frac{1}{2}\rho S C_{L_{max}}}} \tag{3.32}$$

For single engine propeller aircraft $C_{L_{max}}$ ranges from 1.4 to 2.0 [23], and an intermediate approximation is selected to be $C_{L_{max}} = 1.7$ for STARF. The $P_{t,req}$ can be determined by rewriting equation (3.7) for STARF,

$$P_{t,req} = \frac{\frac{1}{2}\rho {V_t}^3 S C_{D_0} + \frac{2(NW)^2 k}{\rho V_t S}}{\eta_{tot}}(1 + DF) \tag{3.33}$$

The load factor N is selected when $P_{t,req} \approx P_{req}$, and is kept under 2.5 as prescribed. Once N is determined, equation (3.30) can be solved to generate r_t.

For X-VERT, FireFLY 6, VOGI and Valkyrie, in order to maximize the bank angle, the turning speed V_t is taken to be the velocity associated with the minimum power consumption during steady level flight, V_P. V_P can be found by plotting P_{req} against V from equation (3.20) and (3.21). The $P_{t,req}$ is determined by performing the calculation procedure depicted by Chapter 3.2.2 and 3.2.3 with W replaced by NW, and N is found when $P_{t,req} \approx P_{req}$ while being kept within the prescribed safety limits.

3.4 Take-off and landing performance evaluation

3.4.1 Non-VTOL aircraft (STARF)

The energy consumption related to STARF's taking-off and ascending, as well as descending and landing is depicted in Fig. 3-10. Energy is conserved during acceleration and deceleration in take-off and landing ground roll, and is again conserved during climbing and descending, where potential energy is firstly raised and then returned. The items to be calculated are losses related to friction and parasite drag forces in different phases.

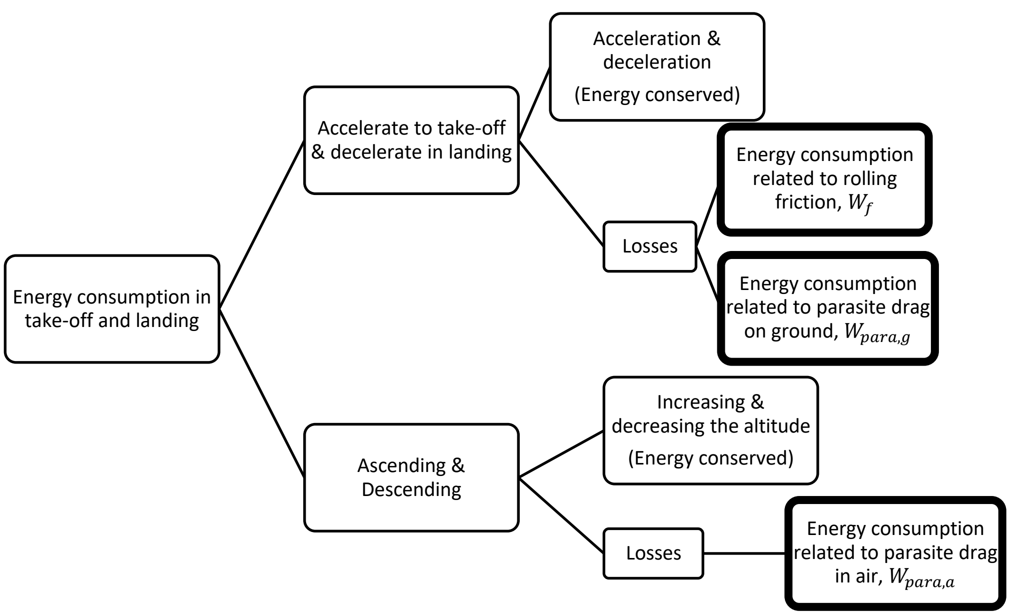

Figure 3-10: Energy consumption associated with take-off and landing, STARF

Note that W_f, $W_{para,g}$ and $W_{para,a}$ calculated in following Chapters 3.4.1.1 and 3.4.1.2 are to be multiplied by 2 to account for total energy losses, assuming take-off and landing to be symmetrical processes.

3.4.1.1 Calculation of W_f and $W_{para,g}$

The evaluation of W_f and $W_{para,g}$ can be derived from Newton's second law of motion,

$$W_f = \int_{l_g=0}^{l_g=l_{g,TO}} \mu_f \left(W - \frac{1}{2}\rho\left[V(l_g)\right]^2 SC_{L,g}\right) \, dl_g \tag{3.34}$$

$$W_{para,g} = \int_{l_g=0}^{l_g=l_{g,TO}} \frac{1}{2}\rho\left[V(l_g)\right]^2 SC_{D_0}(1+DF) \, dl_g \tag{3.35}$$

Where l_g is distance travelled on runway, $C_{L,g}$ is lift coefficient with ground effect incorporated, C_{D_0} is as estimated in Chapter 3.2.1, μ_f is coefficient of rolling friction that typically ranges from 0.02 to 0.1 depending on the surface [13], and an intermediate approximation of 0.06 is adopted. Here a minimized take-off distance is sought, and under this condition integral analysis shows that $C_{L,g}$ is to be adjusted to satisfy [24]:

$$C_{L,g} = \frac{\mu_f}{2k_g} \tag{3.36}$$

Where k_g is the induced drag parameter with ground effect incorporated. The ground effect introduces a correction factor ϕ [13]:

$$\phi = \frac{(16\frac{h}{b})^2}{1 + (16\frac{h}{b})^2} \tag{3.37}$$

Therefore $k_g = \phi k$, where k is calculated as in Chapter 3.2.1, and h and b can be found in Chapter 2.3. The distance required for take-off, $l_{g,TO}$, can be estimated as [13]:

$$l_{g,TO} = \frac{{V_{TO}}^2}{2\bar{a}} \tag{3.38}$$

Where $\bar{a}$ is the average acceleration, or acceleration evaluated at $V_{TO}/\sqrt{2}$. More specifically, $\bar{a}$ can be evaluated as:

$$\bar{a} = \frac{T - \frac{1}{2}\rho\left(\frac{V_{TO}}{\sqrt{2}}\right)^2 S\left[C_{D_0} + k_g {C_{L,g}}^2(1 + DF)\right] - \mu_f\left(W - \frac{1}{2}\rho\left(\frac{V_{TO}}{\sqrt{2}}\right)^2 SC_{L,g}\right)}{m} \tag{3.39}$$

The STARF equips OS 120AX Engine with rated power output of 1.1 HP at 9000 rpm [2], here such constant power is assumed and is used to calculate T under $V = V_{TO}$, with an efficiency of 0.5 as prescribed. The $\bar{a}$ evaluated in equation (3.39) can also be used to generate $V(l_g)$, speed as a function of ground roll distance travelled, by rearranging equation (3.38):

$$V(l_g) = \sqrt{2\bar{a}l_g} \tag{3.40}$$

Finally the take-off speed V_{TO} is to be evaluated based on stall speed, with a safety margin of 20%,

$$V_{TO} = 1.2V_{stall} \tag{3.41}$$

Now the calculation of W_f and $W_{para,g}$ can be performed by substituting equation (3.41) back to equation (3.34) and (3.35).

3.4.1.2 Calculation of $W_{para,a}$

For simplicity, the climbing (or descending) phase is modelled under quasi-steady assumption, that is to keep STARF's airspeed approximately constant at $V = V_{TO}$, with propeller thrust T be kept at same value as in Section 3.4.1.1. An optimization here is decided to be minimizing the airborne distance, which contributes to reducing $W_{para,a}$ losses, by maximizing the climbing angle of attack α_a. The maximized α_a occurs when following is a maximum:

$$sin\,\alpha_a = \frac{T-D}{W} = \frac{T}{W} - \frac{D}{L} = \frac{T}{W} - \frac{C_D}{C_L}$$

The term $\frac{C_D}{C_L}$ reaches minimum at minimum drag condition depicted by equation (3.10), and this leads the max α_a evaluation to be:

$$\alpha_a = \sin^{-1}\left[\frac{T}{W} - \frac{2{C_D}_0}{\sqrt{\frac{{C_D}_0}{k}}}\right] \tag{3.43}$$

Where T is assumed to be the same as in Section 3.4.1.1. As mentioned in Chapter 2.1.1, the recommended height of survey is $H = 30\ m$, therefore the airborne distance and $W_{para,a}$ can be calculated (integration is used for consistency):

$$W_{para,a} = \int_{l_a=0}^{l_a=\frac{H}{\sin\alpha_a}} \frac{1}{2}\rho {V_{TO}}^2 S{C_D}_0(1+DF)\ dl_a \tag{3.44}$$

3.4.2 VTOL aircrafts

By performing take-off and landing vertically, the VTOL platforms (X-VERT, FireFLY 6, VOGI and Valkyrie) are exempt from ground rolling acceleration/deceleration phases. During ascending/descending, the potential energy is again assumed to be conserved as with STARF. The only energy loss item considered is the transitional loss brought by transition from vertical to horizontal (or inverse) flight attitude. Comparing with energy consumed in the full flight envelope, energy losses associated with transient maneuver such as transition is assumed to be negligible.

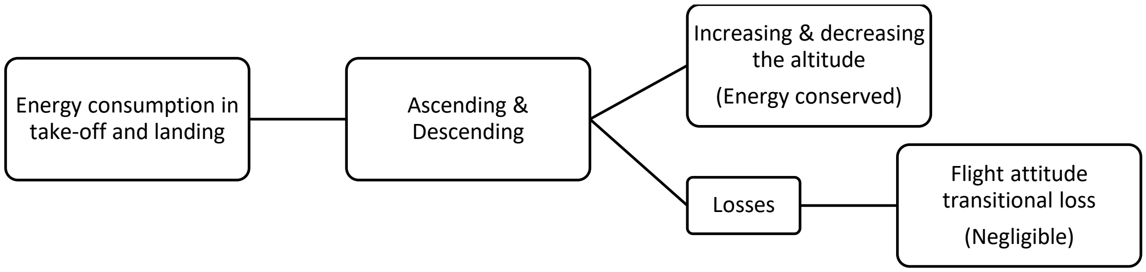

Figure 3-11: Energy consumption associated with take-off and landing, VTOL aircrafts

Chapter 4: Competition results and discussion

This Chapter presents optimal condition flight performance metrics results calculated from Chapter 3. The performance metrics under competition conditions can then be calculated, and they are presented in this Chapter as well.

4.1 Optimal condition flight performance metrics results and discussion

Selected results in diagrams and comprehensive results in tables are presented and discussed in sub-chapters 4.1.1 to 4.1.3.

4.1.1 Valkyrie

For Valkyrie during steady level flight, the power variation with forward speed has been shown in Fig. 4-1. From this diagram it can be seen that the profile power is relatively stable exhibiting only slight increase with speed; the induced power dominates in low flight speed regime and decreases rapidly as speed increases; and parasite power grows proportionally to V^3 from 0 to dominant in high flight speed regime.

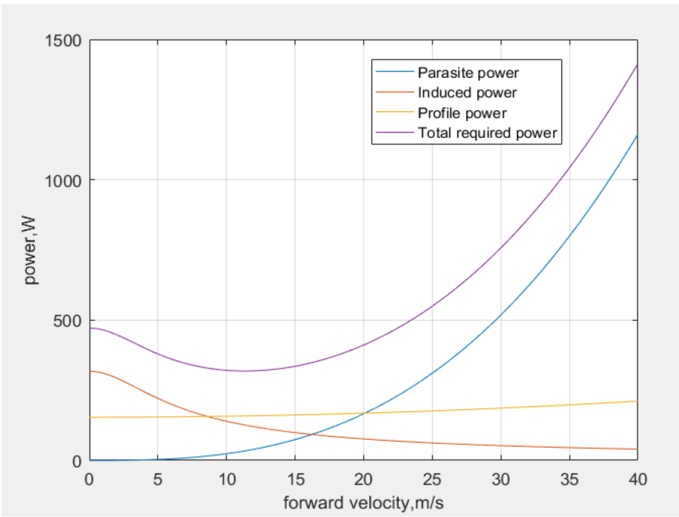

Figure 4-1: Valkyrie, P_{req} breakdown vs V

The range versus velocity diagram is shown in Fig. 4-2, along with the point where maximum range R_{max} occurs.

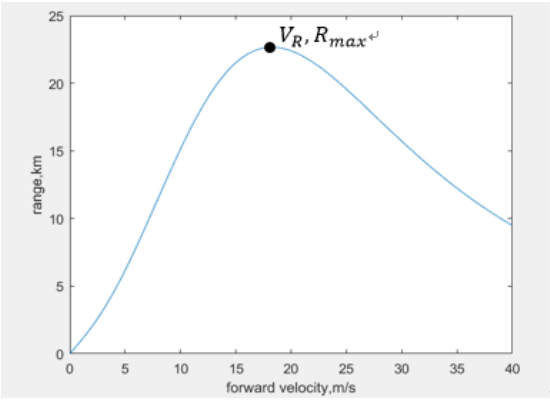

Figure 4-2: Valkyrie, R vs V

4.1.2 Hybrid aircrafts

For VOGI, the resulted range versus velocity diagram is shown in Fig. 4-3. It can be seen that with the presence of a quadrotor airframe, the R vs V diagram shows a similar trend as Valkyrie: flight range increases rapidly as speed approaches V_R, since induced drag effect decreases, or becomes negligible rapidly in this regime; flight range then decreases relatively slowly, as parasite drag increases relatively steadily with speed.

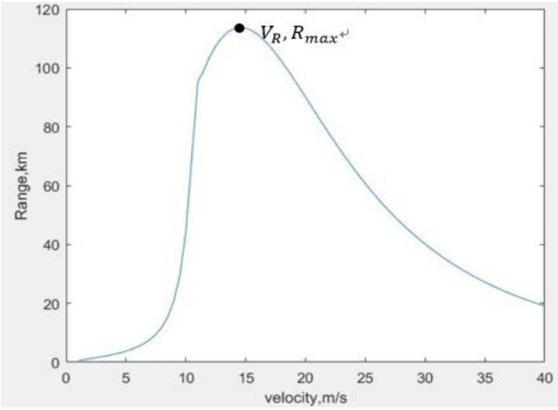

Figure 4-3: VOGI, R vs V

The variation of θ and α with speed has also been plotted in Fig. 4-4 and Fig. 4-5. It can be seen that the aircraft keeps high angle of attack under low speed to compensate the lift, and when it cruises the rotor is rotated to nearly horizontal, with rotor pitch fluctuates around 90°.

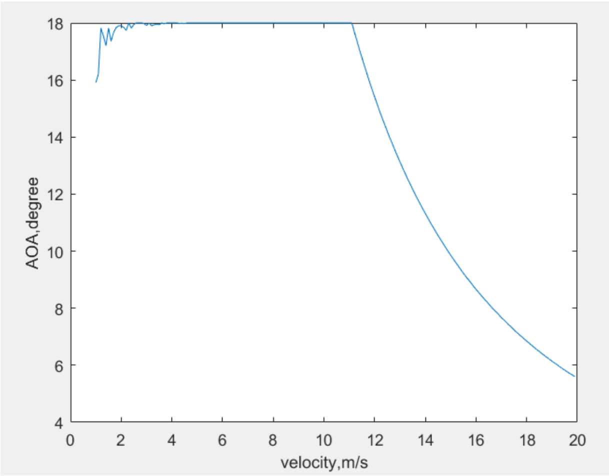

Fig.4-4: VOGI, α vs V

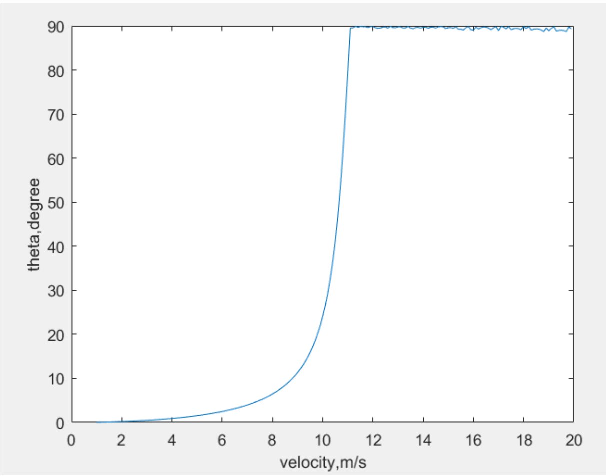

Fig.4-5: VOGI, θ vs V

The α versus V diagram for X-VERT is shown in Fig. 4-6. It shows that when X-VERT is accelerated over certain value of speed and the generated lift outweighs its weight, the aircraft tilt its nose downward exhibiting a negative α to maintain level flight.

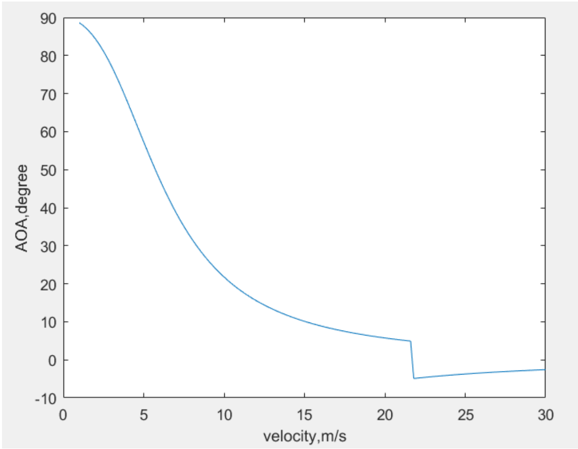

Figure 4-6: X-VERT, α vs V

4.1.3 Comprehensive results

Cruising power and range diagrams for all of the five prototypes are shown in Fig. 4-7 and Fig. 4-8. For STARF, performances are only evaluated from $V = 11\ \mathrm{m/s}$, considering its stall speed given in Table 4-2.

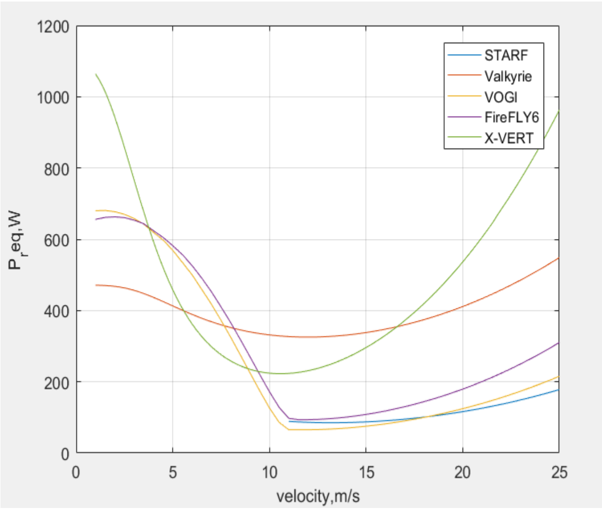

Fig.4-7: All prototypes, P_{req} vs V

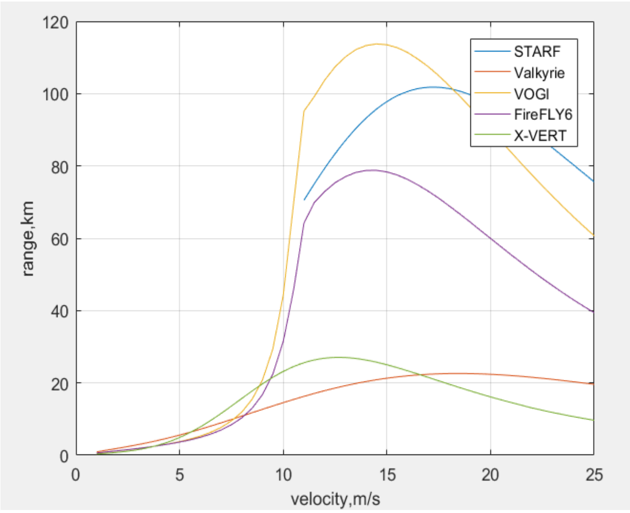

Fig.4-8: All prototypes, R vs V

One conclusion can be drawn from Fig. 4-7 and 4-8 is that the cruising performance of the five prototypes are heavily speed-dependent, with Valkyrie's performance fluctuation with speed being relatively moderate. The performance ranking of these platforms therefore also varies with speed: In a low speed range of 5 m/s to 7 m/s, X-VERT is the most efficient aircraft with the steepest rate of decrease in P_{req} and increase in R; In the speed range of 10 m/s to 17 m/s, where most prototypes reach its optimal performance, VOGI dominates with the lowest P_{req} and highest R, and Valkyrie becomes the worst performed one; In the high speed range of $V > 20$ m/s. where all prototypes' performances with respect to efficiencies drop, VOGI is outperformed by STARF, and X-VERT is outperformed by Valkyrie.

With the above being said, and since the competition #1 depicted in Chapter 2.1.2 actually requires an intermediate cruising speed of 10 m/s to 20 m/s, the comparison will be more comprehensive if the competition #2 is conducted twice in two different flight regime: high speed of 20 m/s, and low speed of 12.8 m/s as limited by 30% safety margin [19] above STARF's stall speed.

In addition, the steep increase in FireFLY 6 and VOGI's flight range in Fig. 4-8 can be explained as a result of the change in their rotor pitching angles, as can be seen in Fig. 4-5. In order to transit from low speed to intermediate speed flight regime with minimized thrust, rotors of VOGI and FireFLY 6 tilt from vertical to horizontal direction. The influence of thrust vectoring over such a wide angle on cruising performance is drastic.

Comprehensive results for all five prototypes are tabulated in Table 4-1. It can be seen that under optimum condition, the hexacopter Valkyrie, as one may expect, has the lowest cruising efficiency evidenced by the largest P_{req} of 378.85 W and smallest R_{max} of 22.65 km among the five prototypes. However, Valkyrie also demonstrates the best maneuverability, evidenced by the shortest r_t of 21.54 m. The CSTT X-VERT exhibits relatively poor performance among hybrid platforms, and possible reasons may include scaling effect and the nature of tail-sitter: The scaling factor for X-VERT (0.3281) has the largest deviation from 1 compared to other prototypes, and such deviation is powered by three and two when scaling W and S, respectively, results in X-VERT's largest weight of $61.41N$ and smallest AR of 3.138. Increase in weight deteriorates X-VERT's performance in an intuitive way that heavier aircraft consumes more power to fly, and decrease in aspect ratio tends to make X-VERT best for swift manoeuvrability but not ideal for sustained endurance flight. The nature of tail sitter refers to X-VERT's tilting mechanism, that unlike tilt-rotor platforms, X-VERT tilts up its nose to acquire more lift with rotors to be pitched at same angle, which reduces rotor thrust in horizontal direction and therefore decreases cruising efficiency. Such speculation can be supported by X-VERT's smallest θ of $76.65°$ among all prototypes measured from true vertical axis.

The tilt-rotor FireFLY 6 consumes more power (112.04 W) and cruises faster (15.42 m/s) compared to the fixed-wing aircraft STARF (98.17 W at 14.57 m/s), and VOGI exhibits better efficiency with less power consumption (72.55 W) at similar cruising speed (14.31 m/s). To have a better investigation and to reach a final conclusion, competitions depicted in Chapter 2.1.2 have to be conducted.

	STARF	X-VERT	FireFLY 6	VOGI	Valkyrie	Unit
DF items	1, 2, 3 (11.99%)	2 (2.76%)	2, 3, 4 (13.14%)	2, 4 (8.71%)	1,3 (9.23%)	-
W	35.51	61.41	47.28	37.86	57.58	N
S	0.351	0.74	0.64	0.325	-	m^2
f_{fuse}	-	-	-	-	0.09	m^2
AR	6.617	3.138	3.629	7.146	-	-
e	0.8365	0.8936	0.8851	0.8284	-	-
k	0.0575	0.1135	0.0991	0.0538	-	-
S_{wet}	1.6848	1.702	2.112	1.0725	0.45 ($S_{wet,fuse}$)	m^2
α	0	13.35	7.86	6.55	2.99	$degree$
θ	90	76.65	89.68	89.49	-	$degree$
Re	1.09e+06	9.87e+05	1.45e+06	6.94e+05	2.31e+05 (Re_{fuse})	-
C_{fe}	0.0065	0.0065	0.0065	0.0065	-	-
C_{D_0}	0.03109	0.0149	0.0213	0.02152	-	-
V_R	14.57	13.40	15.42	14.31	18.27	$\frac{m}{s}$
P_{req}	98.17	246.07	112.04	72.55	378.85	W
$E(V_R)$	1.61	0.58	1.4	2.18	0.34	$hour$
R_{max}	84.41	27.11	77.66	113.74	22.65	km
N	1.06	1.08	1.11	1.1	1.21	-
$P_{t,req}$	96.78	245.06	110.35	71.59	378.52	W
V_t	11.33	10.60	11.50	12.10	12.00	$\frac{m}{s}$
r_t	37.22	28.07	27.98	32.56	21.54	m

Table 4-1: Performance metrics results for all five prototypes under optimal cruising condition

Energy losses in take-off and landing for STARF is tabulated in Table 4-2. It can be seen that the friction loss W_f and parasite drag loss $W_{para,g}$ in ground roll are small enough to be neglected.

V_{stall}	9.856	$\frac{m}{s}$
V_{TO}	11.827	$\frac{m}{s}$
ϕ	0.9317	-
$C_{L,g}$	0.5607	-
$\bar{a}$	8.86	$\frac{m}{s^2}$
$l_{g,TO}$	7.87	m
W_f	12.8	J
$W_{para,g}$	11.73	J
α_a	11.36	$degree$
l_a	154.24	m
$W_{para,a}$	1594.07	J

Table 4-2: Energy losses in takeoff and landing, STARF

4.2 Mission task competition results and discussion

All of the five prototypes are to perform the mission task competitions depicted in Chapter 2.1.2. For competition #1 prototypes are operated under respective optimum conditions presented in Table 4-1, and for competition #2 they will be operated under uniform conditions to be determined later.

In all the competitions the time is started to be recorded once aircraft starts cruising at point A in Fig. 2-1, and ended once aircraft cruises back to point A. Therefore the time consumption in take-off and landing is disregarded, although energy consumption associated with these phases are incorporated as in Table 4-2.

For each comparison criteria described in Chapter 2.1.2 it comes with a performance score q to evaluate it on a quantification basis. The performance score q can be expressed as:

$$q = 10\left(\frac{Aircraft's\ performance\ metric}{Best\ performance\ metric\ of\ all\ five\ aircrafts}\right)$$

Or

$$q = 10\left(\frac{Best\ performance\ metric\ of\ all\ five\ aircrafts}{Aircraft's\ performance\ metric}\right)$$

The selection of either expression depends on which direction (higher or lower) the performance metric can be maximized toward. The overall performance of each prototype is denoted as $Q_{platform}$, which is calculated as the average of q.

4.2.1 Competition #1

The available energy to be consumed for each platform can be calculated as:

$$E_{avail} = (P_{req} + P_{payload} + P_{avionics})E(V_R) \times 0.9$$

A factor of 0.9 is added manually to account for the 10% energy remaining safety margin. The results for competition #1 is tabulated in Table 4-3. Note that the mission task calculation procedure idealized the unsteady process of accelerating to enter the turning and decelerating to exit the turning as a steady one where aircrafts cruise at constant speed $V = V_{cr}$. For each turning, energy change brought by acceleration and deceleration is balanced, however, the total time consumption will be higher than if the steady model is assumed. Therefore, to compensate the time consumption underestimation a 10% addition in time is added to the calculation procedure for all five prototypes in competition #1.

Based on the results presented, the rotary-wing aircraft Valkyrie demonstrates best performance with respect to area ratio and full-envelope average speed, which are results of its shortest radius of turn and highest cruising speed under maximum range condition. However, the power requirement significantly limited its overall performance. In contrast with Valkyrie, the fixed-wing aircraft STARF and tilt-rotor convertiplane FireFLY 6, although demonstrates worse performances with respect to speed and manoeuverability, outperform Valkyrie by having better endurance and efficiency performance, as evidenced by larger observed area and less energy consumption. The X-VERT, as reasoned previously in Chapter 4.1.3, demonstrates the poorest performance in competition #1.

Although VOGI performs relatively poorly with respect to area ratio, its lowest power requirement and therefore best durability make it the best platform for this competition.

	STARF	X-VERT	FireFLY6	VOGI	Valkyrie	Unit
V_{cr} (V_R)	14.57	13.4	15.42	14.31	18.27	$\frac{m}{s}$
V_t	11.33	10.6	11.5	12.10	12.00	$\frac{m}{s}$
r_t	37.22	28.07	27.98	32.56	21.54	m
N	1.06	1.08	1.11	1.1	1.21	-
Turnings performed	59	19	57	83	13	-
Total distance travelled	73.04	25.02	68.03	99.59	17.98	km
Total time consumed	1.43	0.53	1.26	1.96	0.28	hrs
Area observed (q_1)	**2.4 (7.1)**	**0.80 (2.4)**	**2.32 (6.9)**	**3.36 (10)**	**0.60 (1.8)**	km^2
Area ratio (q_2)	**0.54 (5.8)**	**0.72 (7.7)**	**0.72 (7.7)**	**0.62 (6.7)**	**0.93 (10)**	-
Average speed (q_3)	**14.18 (8.0)**	**13.17 (7.4)**	**15.04 (8.4)**	**14.09 (7.9)**	**17.81 (10)**	$\frac{m}{s}$
Energy per distance (q_4)	**8.67 (7.9)**	**20.58 (3.4)**	**9.09 (7.6)**	**6.91 (10)**	**22.66 (3.0)**	$\frac{J}{m}$
$Q_{platform,\#1}$	**7.2**	**5.2**	**7.7**	**8.7**	**6.2**	-

Table 4-3: Competition #1 results

4.2.2 Competition #2

As described in Chapter 4.1.3, the competition #2 is to be conducted in high speed and low speed operation condition with $V_{cr} = 12.8$ m/s and $V_{cr} = 20$ m/s, respectively. With the cruising speed being fixed, calculation procedure described in Chapter 3.2 can be rearranged and performed to generate cruising performance metrics; calculation procedure described in Chapter 3.3 can then be performed to generate turning performance metrics.

To ensure that all prototypes have enough energy to finish the mission task in full length, a conservative number of turnings of 11 is selected by looking at results in competition #1.

4.2.2.1 Competition #2, low speed operation condition

Tabulated results are presented in Table 4-4. In this competition the difference between V_{cr} and V_t is small (ranges from 0.7 m/s to 2.2 m/s), and the time compensation brought by deceleration and acceleration before and after the turning is neglected.

	STARF	X-VERT	FireFLY6	VOGI	Valkyrie	Unit
V_{cr}	12.80	12.80	12.80	12.80	12.80	$\frac{m}{s}$
V_t	11.33	10.6	11.5	12.10	12.00	$\frac{m}{s}$
N	1.01	1.06	1.02	1.02	1.02	-
r_t	92.29	32.58	67.07	74.25	72.03	m
Turnings performed	11	11	11	11	11	-
Total distance travelled	19.21	16.28	17.92	18.28	18.17	km
Total time consumed (q_1)	**0.43 (8.4)**	**0.36 (10)**	**0.39 (9.2)**	**0.40 (9.0)**	**0.39 (9.2)**	hrs
Area ratio (q_2)	**0.23 (3.6)**	**0.63 (10)**	**0.32 (4.9)**	**0.29 (4.6)**	**0.30 (4.8)**	-
Energy per distance (q_3)	**9.21 (7.8)**	**21.19 (3.4)**	**9.53 (7.5)**	**7.19 (10)**	**27.70 (2.6)**	$\frac{J}{m}$
$Q_{platform,\#2,LS}$	**6.6**	**7.8**	**7.2**	**7.9**	**5.5**	-

Table 4-4: Competition #2 low speed results

The above results indicate that for a low speed mission, both X-VERT and VOGI demonstrate decent performances. As with previous competition #1, VOGI demonstrates the lowest power requirement. Although the CSTT X-VERT is fairly inefficient in transit flight reflected by its energy consumption per distance, it demonstrates the shortest time consumption and highest area ratio, which essentially reflects X-VERT's superior manoeuvrability in this speed regime.

For all platforms except X-VERT, it can be seen that their manoeuvrability performances reflected by area ratio decrease drastically as a result of decrease in cruising speed, since a smaller difference between V_{cr} and V_t leads to a smaller N, which then contributes to a longer r_t. Although STARF consumes the most amount of time to finish the competition, its reasonable amount of energy consumption makes it a better platform than Valkyrie for this competition.

4.2.2.2 Competition #2, high speed operation condition

In this competition aircrafts are required to cruise at a speed of $V_{cr} = 20$ m/s. Similar to competition #1, time compensation is required to offset the time deflation results from assuming steady flight before and after each turning. Since the V_{cr} here is higher than those in competition #1, a higher addition rate of 15% instead of 10% is adopted.

	STARF	X-VERT	FireFLY6	VOGI	Valkyrie	Unit
V_{cr}	20.00	20.00	20.00	20.00	20.00	$\frac{m}{s}$
V_t	11.33	10.6	11.5	12.10	12.00	$\frac{m}{s}$
N	1.42	1.66	1.23	1.34	1.32	-
$\boldsymbol{r_t}$ (q_1)	**12.98 (6.6)**	**8.64 (10)**	**18.82 (4.6)**	**16.73 (5.2)**	**17.03 (5.1)**	m
Turnings performed	11	11	11	11	11	-
Total distance travelled	15.47	15.31	15.70	15.62	15.63	km
Total time consumed (q_2)	**0.219 (9.9)**	**0.216 (10)**	**0.225 (9.6)**	**0.222 (9.7)**	**0.222 (9.7)**	hrs
Area ratio	1	1	1	1	1	-
Energy per distance (q_3)	**9.34 (8.2)**	**28.55 (2.7)**	**10.53 (7.3)**	**7.65 (10)**	**22.36 (3.4)**	$\frac{J}{m}$
$Q_{platform,\#2,HS}$	**8.2**	**7.6**	**7.2**	**8.3**	**6.1**	-

Table 4-5: Competition #2 high speed results

With a high cruising speed, all aircrafts demonstrate radius of turn that is shorter than their detection radius (20 m), which then leads to area of 1. Therefore in this competition r_t instead of area ratio is used as one of the evaluation criteria. In addition, it can be seen that for all five prototypes, the difference in total time consumption is relatively minimal, which can also be seen as a result of high cruising speed.

As indicated by the results, VOGI and STARF give satisfactory performance in this competition, where STARF is more maneuverable and VOGI demonstrates the best efficiency. As with competition #2 low speed case, X-VERT demonstrates the highest degree of maneuverability but its overall performance is limited by high energy consumption.

4.2.3 Final overall ranking

	STARF	X-VERT	FireFLY6	VOGI	Valkyrie
$Q_{platform,\#1}$	**7.2**	**5.2**	**7.7**	**8.7**	**6.2**
$Q_{platform,\#2,LS}$	6.6	7.8	7.2	7.9	5.5
$Q_{platform,\#2,HS}$	8.2	7.6	7.2	8.3	6.1
$Q_{platform,\#2}$	**7.4**	**7.7**	**7.2**	**8.1**	**5.8**
$Q_{platform}$	**7.3**	**6.5**	**7.5**	**8.4**	**6**
Ranking	**3**	**4**	**2**	**1**	**5**

VOGI – Naturally, since it aces every competition, the pitch-decoupled tilt rotor platform prototype VOGI becomes the best-performed aircraft in this study. Partial reasons for its performance excellence may derive from its geometrical details: VOGI comes with the lightest weight of 37.86 N among hybrid platforms, and the highest aspect ratio of 7.146 among all platforms. All these factors contribute to a better cruising efficiency.

FireFLY 6 – FireFLY 6 ranks 2^{nd} by keeping stable performances throughout all three competitions. FireFLY 6 demonstrates reasonable amount of energy consumption in optimal, low speed and high speed operation conditions. Although the performance with respect to area ratio/radius of turn drops in competition #2, FireFLY 6's flight efficiency compensates such disadvantage.

STARF – The flight performance of STARF shows a clear increase trend with flight speed, as indicated by STARF's gradual increase in ranking in low speed, optimal, and high speed cases. Another noticeable feature of this fixed-wing aircraft is that STARF's maneuverability performance is more sensitive to change in speed than all the rest prototypes. For instance, under a same V_{cr} increment between competition #2 low speed and high speed cases, STARF demonstrates a largest difference in r_t of 79.31 m. Same conclusion can be drawn if one analyze any two competition cases. Such sensitivity can be explained by STARF's low load factor of 1.06 and 1.01 in competition #1 and #2 low speed case, as from equation (3.30) and (3.31) it can be seen that r_t changes exponentially when N is close to 1.

X-VERT – As previously discussed, X-VERT's low durability and cruise efficiency makes it a non-ideal platform for competition #1. However, in competition #2 such shortcoming is overcome by keeping high degree of agility (ranked 2$^{\text{nd}}$ in $Q_{platform,\#2}$). Although, as told by Fig. 4-7, X-VERT's P_{req} becomes higher than that of Valkyrie as speed increases, the advantage in maneuverability still makes X-VERT a better platform than Valkyrie in this study.

Valkyrie – Apart from poor performance with respect to power requirement, Valkyrie only demonstrates outstanding maneuverability under optimal operating condition. Since Valkyrie's cruising required power P_{req} is relatively insensitive to change in speed, the decrease in r_t is less drastic as speed increases comparing to other platforms.

Chapter 5: Conclusions

As part of this thesis, a framework has been established to compare the flight performances of traditional UAV platforms, represented by fixed-wing and rotary-wing aircrafts, and novel hybrid platforms. The framework includes a flight performance metrics quantification methodology that is developed using a set of assumptions to idealize processes and simplify calculation, and a set of approximations to analytically access aerodynamic coefficients. The framework then generates the performance ranking with respect to the given mission task and operation conditions.

In the standardized competition #2, choices of operating conditions have impacts on aircraft's performance. For instance, in the high speed case where X-VERT ranked 2nd , its overall performance may drop drastically if the speed limit is increased from 20 m/s due to its rapid increase in power requirement with speed as told by Fig. 4-7. Eventually X-VERT will be outperformed by Valkyrie at some high speed point. Similarly, if the safety margin above STARF's stall speed is increased and thereby increasing the low speed limit from 12.8 m/s, STARF's overall performance in competition #2 low speed case can be improved by weakening its disadvantage in maneuverability. Changing the number of turnings to make in competition #2 also influence aircrafts' performance. Assuming power source is switchable, a higher number of turnings than 11 can be achieved by all five prototypes. The increase in turnings will exaggerate the difference in total time consumption in both low speed and high speed cases, and results in improvement of X-VERT's overall performance, since it demonstrates the best performance with respect to total time consumption (q_2) in both cases.

Although VOGI appears to be the best platform in this study, the underlying conclusion drawn is that the performance of aircrafts considered is greatly influenced by their designed parameters.

Since the selection of specific prototype from a platform type is subjective, the results generated from this study does not necessarily indicates the superiority of one platform design over another.

5.1 Future works

To have a more comprehensive examination on aircrafts' maneuverability, one of the future endeavor is to incorporate the ability of hovering into the comparison framework. Such work can be done by evaluating the aircraft's available power and the wind strength it is subject to. The incorporation of hovering ability will have an impact on the final results since it favors the performance of rotorcrafts and hybrid aircrafts.

In addition, in order to generate a more general result that compares the flight performance of different UAV platform designs as listed in Fig. 1-1, one future work to do is to incorporate massive number of prototypes from different platform categories into this framework, and analyze the generated results on statistical basis.

Lastly, a sensitivity study can be conducted to quantitatively investigate how aircrafts' overall performances are influenced by different factors. For example, if the superiority of VOGI's flight performance is deemed to be derived from its designed parameters, then to what point will it be outperformed by other prototype if its weight is increased and aspect ratio is decreased? Similarly, how will X-VERT's performance be influenced if assuming its rotors to be tiltable? Questions in similar manner that aims to investigate influence factors on an isolated basis can be posed in sensitivity study.

List of References

[1] A. S. Saeed, A. B. Younes, S. Islam, J. Dias, L. Seneviratne, and G. Cai, "A review on the platform design, dynamic modeling and control of hybrid UAVs," *2015 International Conference on Unmanned Aircraft Systems (ICUAS)*. IEEE, June 2015, pp. 806–815. [Online]. Available: http://ieeexplore.ieee.org/document/7152365/

[2] Huge, Almost-Ready-to-Fly 8 foot Senior Telemaster ARF available in 2 colors. [Online]. Available: http://www.hobbyexpress.com/srtele_arf.html. [Accessed: 15-Jan-2019]

[3] A. Targui, H. Go et al., "Aero McGill Drones 2017 Design Paper". 2018, McGill University.

[4] C. Romain & M. Nahon (2018). "Modeling and Control of a Tailsitter UAV". 400-409. 10.1109/*ICUAS*.2018.8453301.

[5] Firefly6. Birds Eye View. [Online]. Available: http://www.birdseyeview.aero/products/firefly6.

[6] Apkarian, J. (2018, June). "Attitude Control of Pitch-Decoupled VTOL Fixed Wing Tiltrotor," *2018 International Conference on Unmanned Aircraft Systems (ICUAS)* (pp. 195-201). IEEE.

[7] AI Drone 2017 UAV Competition and Rules (Ver. 1.0) Released February 9, 2017, The University of Tulsa. [Online], Available: https://5ij332mqg4e01sl4ctbg43b5-wpengine.netdnassl.com/wp-content/uploads/sites/4/2017/02/drone-rules-V1-0.pdf. [Accessed: 25-Feb-2019]

[8] R. D. Lorenz, "Flight Power Scaling of Airplanes, Airships, and Helicopters: Application to Planetary Exploration", 2001, University of Arizona, Tucson, Arizona 85721-0092

[9] S. Yadav, M. Sharma, and A. Board. Thrust efficiency of drones (Quad Copter) with different propellers and their payload capacity, *International Journal of Aerospace and Mechanical Engineering*, Volume 4 – No.2, April 2017, ISSN (O): 2393-8609.

[10] Cheng, Heng Teng (2012). "Lead acid batteries modeling and performance analysis of BESS in distributed generation," Other thesis, Murdoch University.

[11] Simpson, C., "Characteristics of Rechargeable Batteries," *National Semiconductor*, Santa Clara, CA, 1995.

[12] Coe Jr, P. L. (1976). “Review of drag cleanup tests in Langley full-scale tunnel (from 1935 to 1945) applicable to current general aviation airplanes”.

[13] McCormick, B. W. (1979). Aerodynamics, aeronautics, and flight mechanics (Vol. 2). New York: Wiley.

[14] Ostler, J. N., “Flight Testing Small Electric Powered Unmanned Aerial Vehicles,” M.S. Thesis, Brigham Young Univ., Salt Lake City, UT, April 2006.

[15] Pixhawk v2 Feature Overview, [Online], Available: https://www.robotshop.com/ca/en/pixhawk-21-standard-set.html. [Accessed: 25-Feb-2019].

[16] Niţă, Mihaela, and Dieter Scholz. Estimating the oswald factor from basic aircraft geometrical parameters. *Deutsche Gesellschaft für Luft-und Raumfahrt-Lilienthal-Oberth eV*, 2012.

[17] H. van Es, Gerard W. "Rapid estimation of the zero-lift drag coefficient of transport aircraft," *Journal of aircraft* 39.4 (2002): 597-599.

[18] Review of aircraft dynamics, Kimerius aircraft, [Online], Available: http://kimerius.com/app/download/5782338201/Review+of+aircraft+aerodynamics.pdf. [Accessed: 12-Feb-2019]

[19] Dhanji, N. (2007). “Comparative Study of Aerial Platforms for Mars Exploration,” (Doctoral dissertation, McGill University).

[20] Test report of MN5212 KV340 motor, [Online], Available: http://store-en.tmotor.com/goods.php?id=377. [Accessed: 02-Feb-2019].

[21] Detailed airfoil characteristic of NACA6409 9%, [Online], Available: http://airfoiltools.com/airfoil/details?airfoil=n6409-il. [Accessed: 02-Feb-2019].

[22] M. Modafferi, M. Quesbel, T. Thompson, P. wilk, “DAN 6: Embodiment Design Report”. 2018, McGill University.

[23] "Part 25 - Airworthiness Standards: Transport Category Airplanes". FAA. Retrieved 29 March 2010.

[24] AOE3104 Vehicle Performance Supplemental Notes: Takeoff & Landing, 2011, Dept. of AOE, Virginia Tech University, [Online]. Available: http://www.dept.aoe.vt.edu/~lutze/AOE3104/. [Accessed: 02-Feb-2019].